

1

The phylodynamic threshold of measurably evolving 2 populations

3 Ariane Weber^{1,*}, Julia Kende^{2,3}, Camila Duitama González^{3,4}, Sanni Översti^{1,‡} and Sebastian
4 Duchene^{3,4,5,‡,*}.

5

6 ¹ Max Planck Institute of Geoanthropology, Jena, Germany.

7 ² Bioinformatics and Biostatistics Hub, Institut Pasteur, Paris, France.

8 ³ Université Paris Cité, Paris, France.

9 ⁴ ED-ID unit, Dept of Computational Biology, Institut Pasteur, Paris, France.

10 ⁵ Peter Doherty Institute for Infection and Immunity, Dept of Microbiology and Immunology, University
11 of Melbourne, Melbourne, Australia.

12 *email: weber@gea.mpg.de, sduchene@pasteur.fr

13 ‡ Equal contribution to the supervision of this work.

14

15 **Abstract** The molecular clock is a fundamental tool for understanding the time and pace of evolution,
16 requiring calibration information alongside molecular data. Sampling times are often used for calibration since
17 some organisms accumulate enough mutations over the course of their sampling period. This practice ties
18 together two key concepts: measurably evolving populations and the phylodynamic threshold. Our current
19 understanding suggests that populations meeting these criteria are suitable for molecular clock calibration
20 via sampling times. However, the definitions and implications of these concepts remain unclear. Using
21 Hepatitis B virus-like simulations and analyses of empirical data, this study shows that determining whether
22 a population is measurably evolving or has reached the phylodynamic threshold does not only depend on the
23 data, but also on model assumptions and sampling strategies. In Bayesian applications, a lack of temporal
24 signal due to a narrow sampling window results in a prior that is overly informative relative to the data,
25 such that a prior that is potentially misleading typically requires a wider sampling window than one that
26 is reasonable. In our analyses we demonstrate that assessing prior sensitivity is more important than the
27 outcome of tests of temporal signal. Our results offer guidelines to improve molecular clock inferences and
28 highlight limitations in molecular sequence sampling procedures.

29 **Keywords:** Measurably evolving population, phylodynamic threshold, molecular clock, Bayesian phylo-
30 genetics, microbial evolution.

31

1 Introduction

32 Molecular sequence data have become nearly ubiquitous for studying the evolution of modern and ancient
33 organisms. A fundamental concept in molecular evolution is the ‘molecular clock’, which posits that substitu-
34 tions accumulate roughly constantly over time (Zuckerkandl and Pauling, 1965). An underlying assumption
35 of the classic molecular clock is that selective constraints are negligible for most sites and over time. The
36 development of molecular clock models as statistical processes relaxes this and other assumptions by allow-
37 ing for rate variation among branches (and sometimes sites see Ho 2014) in phylogenetic trees (reviewed by
38 Guindon (2020), Ho and Duchêne (2014)).

39 Molecular clock models necessarily involve two key quantities, the evolutionary timescale and the ‘evolu-
40 tionary rate’, with the latter representing the combination of mutations and substitutions that accrue over
41 time. However, evolutionary times and rates are unidentifiable (Dos Reis and Yang (2013), as reviewed by
42 Bromham et al. 2018, Guindon 2020), and therefore cannot be jointly estimated using genetic sequence data
43 alone. To make inferences from genetic sequences, all molecular clock methods require prior assumption
44 about evolutionary times or rates, known as a ‘molecular clock calibration’. Three main calibrations exist:
45 First, the age of the most recent common ancestor between two samples can be constrained to a given time
46 point or interval (‘internal node calibration’). Second, a known estimate of the evolutionary rate can be in-
47 corporated (e.g. as a prior in Bayesian frameworks). Third, in cases where molecular sequences are sampled
48 at different points in time (heterochronous sampling), the tips of the phylogeny can be anchored to these
49 time points (‘tip calibration’; reviewed by Rieux and Balloux (2016)). The choice of calibration depends on
50 the information available and its reliability (Duchêne et al., 2014, Warnock et al., 2012). For instance, it
51 would be remiss to ignore evidence about when two lineages shared a common ancestor if the fossil record
52 is compelling (Gavryushkina et al., 2017, Ronquist et al., 2016). Crucially, multiple sources of calibration
53 information can be provided for the molecular clock.

54 1.1 Measurably evolving populations

55 Rapidly evolving organisms, notably many viruses and bacteria, have been found to accrue an appreciable
56 number of mutations over the sampling timescale. Influenza viruses, for example, have evolutionary rates
57 of around 6×10^{-3} subs/site/year (substitutions per genomic site per year) (Ghafari et al., 2022, Sanjuán,
58 2012). Assuming a genome size of 13,500 nucleotides, one would expect to observe one mutation every 4 to
59 5 days ($\frac{365 \text{ days/year}}{13,500 \text{ sites} \times 6 \times 10^{-3} \text{ subs/site/year}} \approx 4.5 \text{ days/subs}$). If genome samples are collected over the course of
60 a few weeks, the sampling times themselves can be used to calibrate the molecular clock and tip calibration
61 is therefore warranted. Data sets for which tip calibration is feasible are considered to have been sampled
62 from a ‘measurably evolving population’ (Drummond et al., 2003b) and to have ‘temporal signal’.

63 Measurably evolving populations are typically characterised either by a sampling period that is long
64 relative to the evolutionary rate, a sufficiently big data set (long molecular sequences or many samples), or
65 both. Traditionally, such characteristics were mainly found in rapidly evolving organisms, typically RNA
66 viruses. Nowadays, advances in sequencing technologies have dramatically expanded the range of organisms
67 from which data sets can be considered to have been sampled from a measurably evolving population.
68 Namely, ancient DNA techniques have effectively expanded the genome sampling window for many organisms
69 (Duchene et al., 2020b, Spyrou et al., 2019a), and whole genome sequencing has meant that data sets of
70 ‘slowly’ evolving microbes often carry sufficient information for calibrating the molecular clock (Biek et al.,
71 2015) even when the sampling period covers only a few decades (Menardo et al., 2019).

72 1.2 The phylodynamic threshold

73 Genomic data sets collected during the early stages of an outbreak, for example, often pose two problems: low
74 genetic diversity and a narrow sampling window. Both can lead to highly uncertain estimates of evolutionary
75 rate and time of origin. The point at which an organism has accumulated sufficient genetic changes since its
76 emergence to allow for informative tip calibration is referred to as the ‘phylodynamic threshold’ (Duchene

77 et al., 2020a). At a minimum, tip calibration requires that one mutation has occurred over the sampling period
78 for the method to be informative. For a given organism, the minimum sampling period can be calculated as the
79 inverse of the product of genome size and the evolutionary rate (i.e. $\frac{1}{\text{genome size (sites)} \times \text{evol. rate(subs/site/year)}} =$
80 years to observe one mutation). We refer to this amount of time as the expected phylodynamic threshold.

81 The terms phylodynamic threshold and measurably evolving population are different, albeit related,
82 concepts. A population is measurably evolving if the samples available are sufficiently informative as to allow
83 for tip calibration. In contrast, the phylodynamic threshold is the amount of time over which we would
84 need to draw samples after their emergence for them to behave as from a measurably evolving population.
85 For a recently evolving pathogen the phylodynamic threshold would simply correspond to the time until it
86 can be considered a measurably evolving population, under the condition that the data have been collected
87 constantly over time. In contrast, an organism that emerged further in the past may have accumulated
88 considerable genetic diversity over time, effectively reaching its phylodynamic threshold. However, if samples
89 are drawn from a very short time window they may fail to capture a representative amount of such genetic
90 diversity.

91 1.3 Tests of temporal signal

92 Our ability to extract information from a tip calibration framework can be assessed through tests of temporal
93 signal. The importance of performing such tests arises from the observation that a lack of temporal signal
94 is associated with unreliable evolutionary rate estimates (Duchêne et al., 2015, Rieux and Balloux, 2016),
95 although the presence and direction of a potential bias remain poorly understood. However, it is important to
96 note that a lack of temporal signal does not necessarily preclude estimating evolutionary rates and timescales
97 because alternative sources of calibration, such as prior estimates of evolutionary rates or constraints on
98 internal node ages, can still be used to inform analyses.

99 In principle, frameworks developed to test for temporal signal do not differentiate between recently
100 emerging organisms (fig. 1a) and those with narrow sampling windows (fig. 1d), both of which may lack
101 temporal signal. As most of these tests involve fitting a phylogenetic model to the data, they implicitly
102 assume that the model adequately captures the evolutionary process and thus their performance also highly
103 depends on model fit. Recent research, for example, suggests that the choice of tree prior and molecular
104 clock model significantly impacts the sensitivity and specificity of temporal signal tests (Tay et al., 2024).
105 Thus, temporal signal is not solely a property of the data but also depends on the choice of model.

106 Various methods exist for assessing temporal signal. The root-to-tip regression (Buonagurio et al., 1986,
107 Drummond et al., 2003a, Gojobori et al., 1990) fits a regression to the distance from the root to the tips in a
108 phylogenetic tree against sampling time. High R^2 values of the regression suggest that phylogenetic distance
109 can be sensibly modelled as a linear function of time and can thus be used as an indication of informative
110 tip-calibration. Date-randomisation tests (Duchêne et al., 2015, Duchene et al., 2018, Ramsden et al., 2009,
111 Trovão et al., 2015) compare evolutionary rate estimates using correct sampling times against those from
112 permutations. Bayesian Evaluation of Temporal Signal (BETS; Duchene et al. (2020c)) evaluates whether
113 a model with sampling times performs better than a model that assumes isochronous sampling using Bayes
114 factors. Each method comes with a set of limitations and strengths, such that tests of temporal signal should
115 rather be used in combination than being mutually exclusive (Duchene et al., 2020c, Rieux and Balloux,

116 2016).

117 **1.4 Concepts of measurably evolving populations, the phylodynamic threshold, and**
118 **temporal signal in practice**

119 In fig. 1, we present four simple example cases to illustrate the relationships among the concepts of mea-
120 surably evolving populations, the phylodynamic threshold, and temporal signal. The first example depicts
121 an organism that has emerged recently and therefore has not yet reached its phylodynamic threshold (with
122 a phylogenetic time tree shown in panel (a)). Due to its recent origin, there has not been enough time for
123 the accumulation of a sufficient number of substitutions (represented in the phylogram in panel (b)), such
124 that it is not possible to establish a statistical relationship between molecular evolution (i.e., substitutions)
125 and time (as shown in panel (c)). A real-world example of such a case comes from the early phase of the
126 SARS-CoV-2 outbreak: initial efforts to estimate the evolutionary rate and time of origin had substantial
127 uncertainty due to a narrow sampling window and low genetic diversity (Boni et al., 2020). In Duchene et al.
128 (2020a), Bayesian phylodynamic analyses were conducted on genome data as the outbreak unfolded. The
129 number of available genomes and the width of the sampling window increased over time and ranged from
130 22 genomes sampled over 31 days to 122 genomes sampled over 63 days. Although early estimates of the
131 evolutionary rate and time of origin were highly uncertain, they quickly converged to stable values as more
132 data became available (Ghafari et al., 2022).

133 The second example in fig. 1 illustrates a case in which an organism has evolved over a long period,
134 but the available sequence data have been collected within a very narrow timeframe, insufficient to treat the
135 dataset as a measurably evolving population (time tree in panel (d) and phylogram in panel (e)). This results
136 in no temporal signal, as demonstrated by the lack of correlation in the root-to-tip regression in panel (f).
137 The causative agent of tuberculosis, the bacterium *Mycobacterium tuberculosis*, was commonly considered to
138 evolve too slowly for calibrating the molecular clock using samples collected over a few years Duchene et al.
139 (2016). A range of studies have shown, however, that for *M. tuberculosis* a genome sampling window of a few
140 decades might be sufficient for reliable clock calibration (Eldholm et al., 2015, Kühnert et al., 2018, Menardo
141 et al., 2019, Merker et al., 2022).

142 The third example in fig. 1 describes a data set that may involve a wide sampling window of time and
143 for which samples have been drawn from a population that has attained its phylodynamic threshold, but
144 with substantial rate variation among lineages – i.e. overdispersed molecular clock -, resulting in a lack of
145 temporal signal (panels (g) – (i)). This pattern appears to be the case in *Yersinia pestis*, the bacterium
146 that causes the plague, for which some localised outbreaks display obvious temporal signal, but its long-term
147 evolution has pervasive evolutionary rate variation (Andrades Valtueña et al., 2022, Eaton et al., 2023).

148 In the final example in fig. 1, a hypothetical organism has attained its phylodynamic threshold, has been
149 sampled for sufficiently long time, and evolutionary rate variation among lineages is low. These conditions
150 together produce a clear relationship between molecular evolution and time, thus providing unequivocal
151 temporal signal (panels (j) – (l)). The long term evolution of *Vibrio cholerae*, the causative agent of cholera,
152 and H3N2 influenza virus are exemplar microbes whose molecular evolution has been fairly constant across
153 long periods of time (Devault et al., 2014, Rambaut et al., 2016).

154 In summary, the concepts of measurably evolving population, phylodynamic threshold and temporal signal

155 describe the information that can be drawn from a sampled population about its evolutionary timescale.
156 Because populations that are not measurably evolving have been observed to yield biased estimates, they
157 remain important to consider (Gharbi et al., 2024). In Bayesian inference, such biases can be the result
158 of complex interactions between prior distributions or model settings that do not align with the true data
159 generating model, as these drive the inference in the absence of informative data. Traditionally, potential
160 biases due to prior interactions (Tay et al., 2024) or model misspecification (Möller et al., 2018) have been
161 found through simulations studies, while data analyses often involve little validations of the results (Mendes
162 et al., 2025). Here, we illustrate through a range of examples the degree to which differing levels of temporal
163 signal in a data set can interact with prior settings and model assumptions, both on simulated and empirical
164 data.

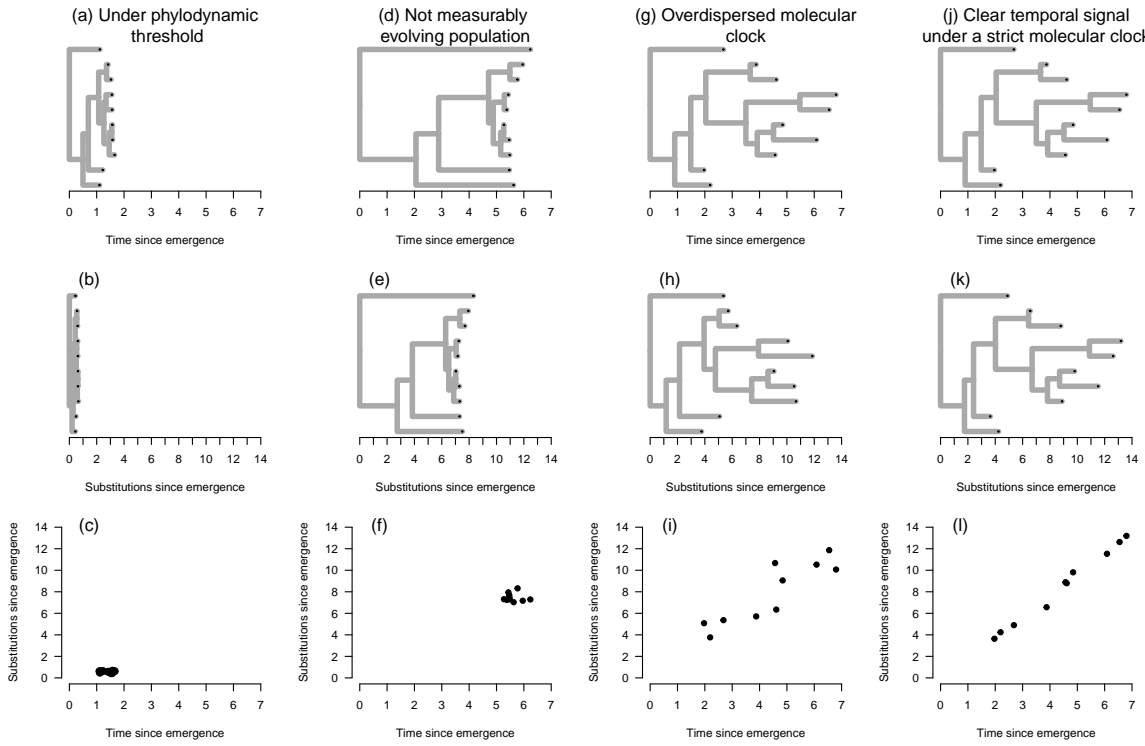


Figure 1: Examples of situations where temporal signal may or may not be detected. An organism that has not attained its phylodynamic threshold has a recent time of emergence (with a phylogenetic time tree shown in (a)) because it has not had sufficient time to accrue an appreciable number of substitutions (phylogenetic tree with branch lengths in subs/site, i.e. a ‘phylogram’, shown in (b)), such that it is not possible to establish a statistical relationship between molecular evolution (substitutions) and time (shown in (c)). Sequence data from an organism that has evolved for a substantial amount of time may have been sampled over a very narrow window of time that is not sufficient to treat it as a measurably evolving population (time tree in (d) and phylogram in (e)), which results in no temporal signal (root-to-tip regression in (f)). A data set may involve a wide sampling window of time and from a population that has attained its phylodynamic threshold, but an overdispersed molecular clock (substantial rate variation among lineages; panels (g) - (i)) may result in a lack of temporal signal. In (j) through (l) we show the situation where an organism has attained its phylodynamic threshold, it has been sampled for sufficiently long, and where evolutionary rate variation among lineages is negligible, as to produce a clear relationship between molecular evolution and time, and thus unequivocal temporal signal.

165 **2 Results**

166 We sought to pinpoint the impact of sampling strategies on molecular clock estimates. We focused our attention
167 on two major problems for emerging microbes and studies involving ancient DNA. First, we conducted
168 simulations varying the sampling window of a population that had attained its phylodynamic threshold. In
169 the second simulation scenario, we subsampled a population over time to vary the number of ancient samples,
170 leading to a temporal sampling bias. Finally, we illustrate these results in an empirical data set of Hepatitis
171 B virus (HBV) that includes a large number of ancient samples (Kocher et al., 2021). This virus has been
172 the subject of intense research due to its close association with human populations and complex evolutionary
173 dynamics (Kahila Bar-Gal et al., 2012, Paraskevis et al., 2013, Ross et al., 2018).

174 **2.1 Sampling windows relative to the phylodynamic threshold**

175 We simulated sequence data that resembled the evolution of HBV, a double-stranded DNA (dsDNA) virus
176 that has evolved in humans at least for around ten thousand years (Kocher et al., 2021). Our synthetic
177 data had a genome length of 3,200 nucleotides and an evolutionary rate of 1.5×10^{-5} subs/site/year
178 (Kocher et al., 2021, Mühlemann et al., 2018) with a moderate amount of rate variation among lineages
179 (see Materials and methods). Under these conditions we expect to observe one mutation every 20 years
180 ($\frac{1}{3,200 \text{ sites} \times 1.5 \times 10^{-5} \text{ subs/site/year}} \approx 20 \text{ years/subs}$). This number is important for the design of our simulation
181 experiments: 20 years is the expected phylodynamic threshold, as introduced above, and typically serves
182 as a good reference point from when on to expect temporal signal. We analysed the data under a Bayesian
183 phylogenetic framework and considered whether the posterior contained the true value used to generate the
184 data, known as coverage, and the width of the posterior, known as precision (a precise estimate has a narrow
185 posterior distribution).

186 We conceived a simulation process under which the evolutionary timescale had an expectation of ten
187 thousand years and with a sampling window of 0, 10, 20, 200 , or 2,000 years. A sampling window spanning
188 0 years results in ultrametric trees with the sampling times providing no calibration information. In contrast,
189 a sampling window of 10 years is half of the expected phylodynamic threshold and is likely to have weak
190 temporal signal (see fig. 1(d)-(f)). Sampling windows of 20 years (the expected phylodynamic threshold)
191 or wider are more likely to behave as measurably evolving populations with increasingly strong temporal
192 signal (see fig. 1(j)-(l)). Our synthetic data sets were analysed under Bayesian phylogenetic framework, as
193 implemented in the BEAST 2 platform (Bouckaert et al., 2019).

194 To investigate the impact of the prior we considered several configurations for the prior on the mean
195 evolutionary rate. In our analyses the molecular clock model is a uncorrelated relaxed molecular clock model
196 with an underlying lognormal distribution, with mean M . For this parameter we set nine possible prior
197 Gamma distributions, for which the prior mean could be the value used to generate the data, or one order of
198 magnitude higher or lower. We also included three degrees of uncertainty in this prior (see fig. 2 and table
199 ??). In this respect, a prior with low uncertainty, and a mean that is much higher or lower than the true
200 should result in more bias than one that has higher uncertainty or is centred on the true value.

201 Our simulations for which the prior on M was centred on the true value had very high coverage. At
202 least 94 out of 100 simulation replicates across sampling windows included the true value of M within their

203 95% credible interval (CI) (table ?? and fig. 2). Coverage, however, was associated with the degree to
204 which the prior was biased and the sampling window width. For example, when the prior was highly precise
205 (95% CI/mean=1.0) but biased downwards, even the simulations with a sampling window of 100× the
206 phylodynamic threshold (i.e. 2,000 years before present) still had low coverage (only 1 out of 100 simulation
207 replicates included the true value in the 95% credible interval, table ??).

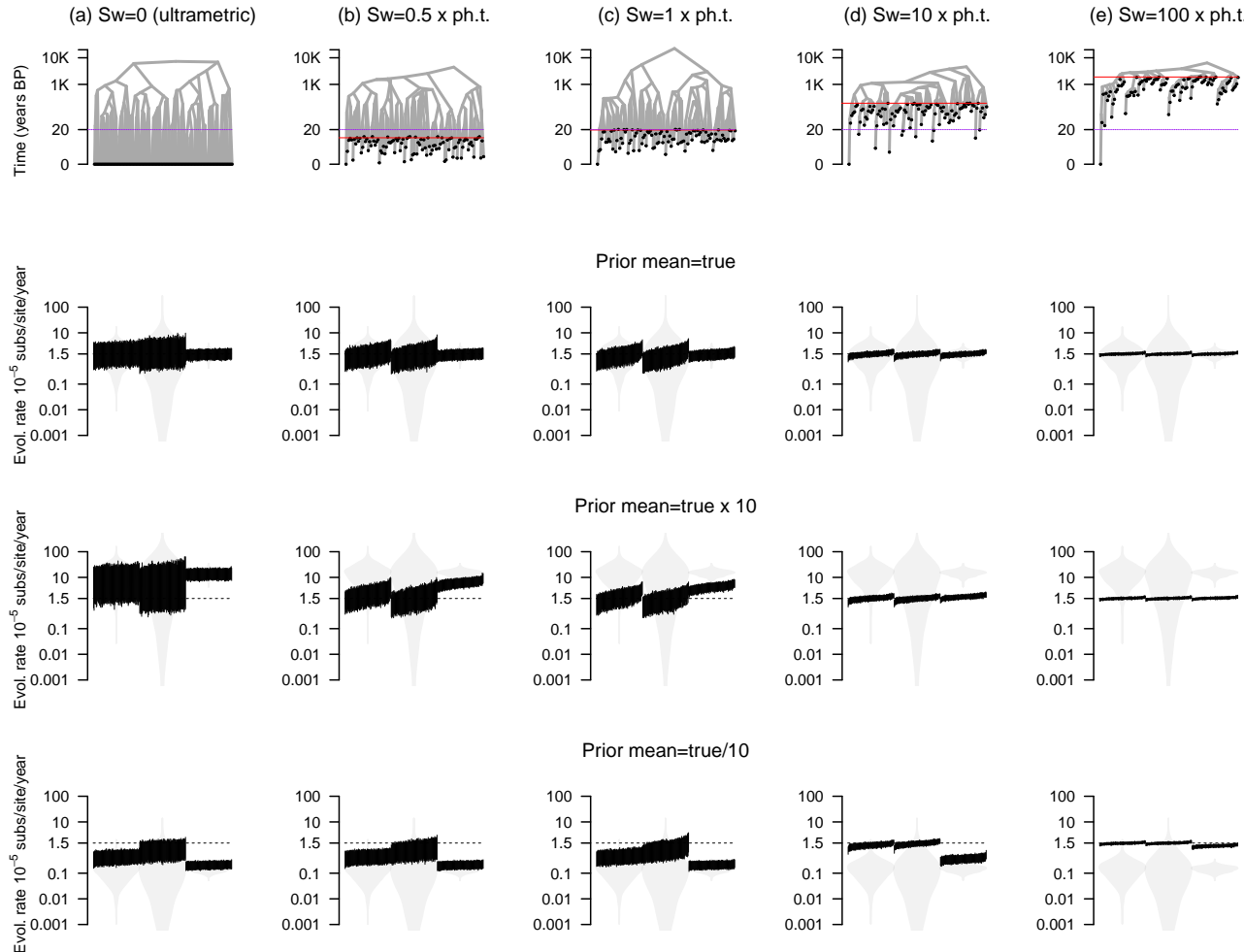


Figure 2: Estimates of evolutionary rates, M for simulations of varying sampling window widths. Each column corresponds to a simulation setting: (a) is for ultrametric trees where all samples are collected at the same point in time (sampling window, $sw=0$), (b) is for the situation where the sampling window is 10 years (half the expected phylodynamic threshold; sampling window, $sw=0.5 \times \text{ph.t.}$), (c) is where the sampling window is exactly the expected phylodynamic threshold of 20 years ($sw=1 \times \text{ph.t.}$). Scenarios (d) and (e) denote sampling windows that are 10 and 100 \times the expected phylodynamic threshold ($sw=10 \times \text{ph.t.}$ and $sw=100 \times \text{ph.t.}$, respectively). The rows denote example phylogenetic trees and prior configurations where the mean is set to the correct value (first row), an order of magnitude higher (second row), or an order of magnitude lower, last row). The prior is shown with the grey violins and each black bar is the 95% credible interval of the posterior. The dashed line in each case denotes the correct value.

208 The uncertainty in estimates of evolutionary rates was associated with the width of the sampling win-
209 dow, but also with the uncertainty in the prior. In the situation where the sampling window was $1\times$ the
210 phylodynamic threshold or less we consistently found that uncertainty in the prior was commensurate with
211 uncertainty in the posterior. Estimates using a prior uncertainty of 1.00 (the width of the 95% credible
212 interval is the same as the mean) are narrower than those using a prior of uncertainty of 3.04 or 6.33 (see
213 table ?? and fig. 2).

214 When the sampling window was $10\times$ the phylodynamic threshold or more we found a more complicated
215 picture. When the prior had a downward bias (mean= 1.5×10^{-6} subs/site/year) and a narrow credible interval
216 of 1.00, the posterior estimate was wider than when this prior was less uncertain (table ?? and fig. 2). This
217 finding can be explained because a very wide sampling window provides a large amount of information for
218 inferring the evolutionary rate, which can yield high uncertainty if the prior stands in conflict. Importantly,
219 the widest sampling window in our experiments, of $100\times$ the phylodynamic threshold produced consistently
220 high precision, although it is important to note that when the prior is highly biased downward (mean of
221 1.5×10^{-6} subs/site/year and uncertainty of 1.00) coverage is very low, with only one simulation replicate
222 containing the true value used to generate the data within the 95% credible interval.

223 To understand the directionality of posterior evolutionary rate estimates relative to the value used to
224 generate the data, we quantified the amount of bias, as difference between the true evolutionary rate and the
225 posterior mean divided by the true value (i.e. $\frac{\text{true value} - \text{posterior mean}}{\text{true value}} = \frac{1.5 \times 10^{-5} - \text{posterior mean}}{1.5 \times 10^{-5}}$). As expected,
226 when the prior was centred in the true value, we observed no or minimum bias, with values ranging from an
227 average of 0.00 and 8.31 (a posterior estimate that was on average 8 times higher than the truth). The most
228 marked average bias was found for our prior with mean 1.5×10^{-4} subs/site/year and an uncertainty of 1.00,
229 which could be as high as 8.31 (table ??). Increasingly wide sampling windows had lower amounts of bias.
230 A sampling window of $100\times$ the phylodynamic threshold had a maximum average bias of -0.22 for the prior
231 with downward bias and low uncertainty, with other prior configurations resulting in a bias of at most -0.22.

232 Overall, these simulations demonstrate that increasingly wide sampling windows result in evolutionary
233 rate estimates that are more accurate, precise, and less biased, than those from data sets with narrow sam-
234 pling windows. Although increasingly wide sampling windows are more robust to prior misspecification, we
235 emphasise the importance of choosing the prior for this parameter carefully. Contrary to the expectation that
236 low temporal signal necessarily results in an underestimation of the evolutionary rate and an overestimation
237 of the tree height (Duchêne et al., 2015), we find that a lack of temporal signal due to narrow sampling
238 windows may simply lend more influence to the prior.

239 For all trees that were non ultrametric (i.e. those with a sampling window width of at least $0.5\times$ the
240 phylodynamic threshold) a downward bias in the evolutionary rate prior appears to be more detrimental
241 than one with an upward bias. In our simulations with sampling windows of width $100\times$ the phylodynamic
242 threshold a highly biased prior (mean= 1.5×10^{-6} subs/site/year and uncertainty of 1.00) still had very low
243 coverage. In contrast, a prior with a similar upward bias (mean= 1.5×10^{-4} and uncertainty of 1.00) produced
244 much higher coverage for sampling windows from $10\times$ the phylodynamic threshold (table ??).

245 These results indicate that priors with high uncertainty should be advised for practical studies. In our
246 simulations posterior estimates using a prior uncertainty of 6.33 seemed to produce a good trade-off between
247 uncertainty and accuracy. Such a prior means that the 95% credible interval spans just over six orders

248 of magnitude. For a sampling window of $1\times$ the phylodynamic threshold, the posterior distribution had
249 an average uncertainty of around 1.7, which may be sufficient for biological interpretation of estimates of
250 evolutionary rates and timescales.

251 **2.2 Hierarchical priors and the phylodynamic threshold**

252 An attractive approach for specifying prior distributions for parameters that are largely unknown is to use a
253 hierarchical structure, where the parameters that govern the prior have priors themselves (sometimes known
254 as hyperpriors). In the context of Bayesian molecular clocks, such hierarchical structure has been used to
255 specify uncertainty in time calibrations ((Heath et al., 2014)). We employed this method by setting a prior
256 for the shape and rate parameters of the Gamma distribution that governs the evolutionary rate, M (see
257 Materials and methods).

258 Under the hierarchical structure, the marginal prior for M is very uncertain and is biased upwards,
259 relative to the true value (fig 3). However, for sampling windows of at least $1\times$ the phylodynamic threshold
260 its performance in terms of coverage, average uncertainty, and average bias were comparable to those using
261 the standard prior centred on the correct value (see first three rows under SW= $1\times$ in tables ??, ??, and ??,
262 compared to table ??). This result demonstrates the effect of Bayesian regularisation and suggests that such
263 hierarchical structure is likely preferable to using a prior that is potentially highly biased.

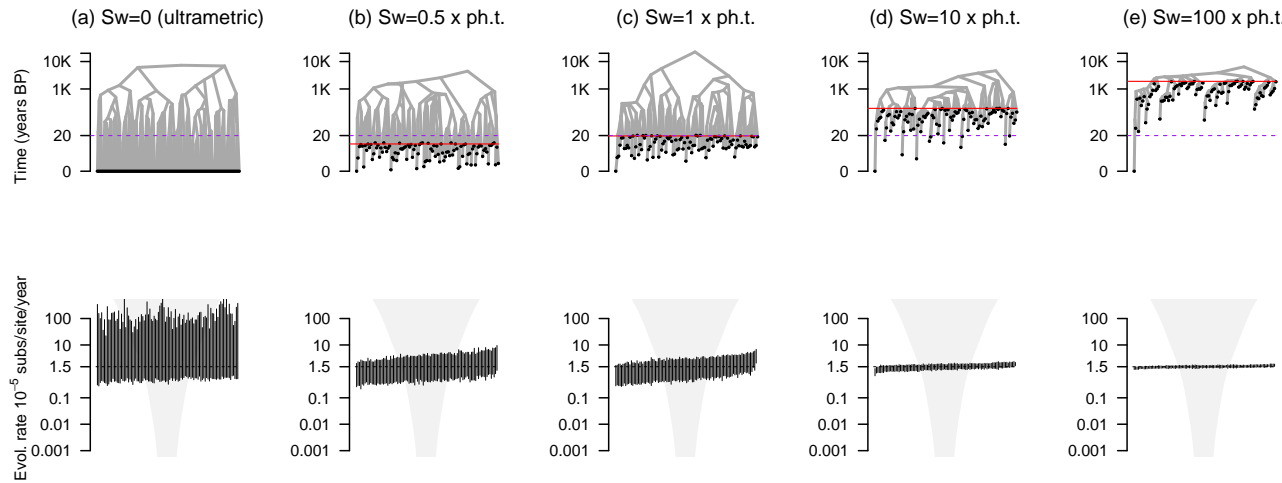


Figure 3: Estimates of evolutionary rates, M for simulations of varying sampling window widths. Each column corresponds to a simulation setting: (a) is for ultrametric trees where all samples are collected at the same point in time (sampling window, $sw=0$), (b) is for the situation where the sampling window is 10 years (half the expected phylodynamic threshold; sampling window, $sw=0.5 \times \text{ph.t.}$), (c) is where the sampling window is exactly the expected phylodynamic threshold of 20 years ($sw=1 \times \text{ph.t.}$). Scenarios (d) and (e) denote sampling windows that are 10 and 100 \times the expected phylodynamic threshold ($sw=10 \times \text{ph.t.}$ and $sw=100 \times \text{ph.t.}$, respectively). The first row denotes example phylogenetic trees, while the second row is the corresponding posterior estimates. The prior is shown with the grey violins (a hierarchical prior configuration) and each black bar is the 95% credible interval of the posterior. The dashed line in each case denotes the correct value.

264 **2.3 Temporal sampling bias**

265 We investigated the impact of temporal sampling bias on the precision and accuracy of molecular clock
266 estimates. For this purpose we simulated data with the same genomic characteristics as HBV and where
267 genome sampling was conducted over five periods of time uniformly distributed between the present and the
268 root of the trees (fig. 4(a)). The fully sampled trees contained 500 genome samples, with 100 for each of
269 the five sampling times. Such stratified sampling is expected in ancient DNA studies, for example when a
270 set of samples are drawn from archaeological sites (e.g. Spyrou et al. (2019b)). We sampled the complete
271 data sets by randomly selecting 20 samples from each strata, which we refer to as ‘time-uniform’ sampling,
272 and by sampling with a probability that is inversely proportional to the age of the strata, referred to as
273 ‘time-biased’. The time-uniform and time-biased sampling strategies both contain 100 samples (1/5th of the
274 complete data), but the time-biased only includes a small number of ancient samples.

275 The coverage of the evolutionary rate estimate was comparable across simulation treatments (table ??). It
276 is worth noting that the coverage and other performance metrics were lower than for our simulation treatment
277 where samples are uniformly drawn between the phylodynamic threshold and the present, which likely occurs
278 because in this case samples with identical sampling times form monophyletic groups, reducing the amount
279 of temporal information in the data (see (Murray et al., 2016) for a detailed investigation). Our measures of
280 coverage and average bias did not differ substantially between sampling treatments.

281 A striking result of the temporal sampling strategies was its impact in uncertainty of the posterior. Both,
282 the time uniform and time-biased sampling treatments resulted in posterior distributions that were wider
283 than with the complete data, which is to be expected because they are effectively smaller data sets with
284 less information, but no systematic bias (fig. 5(a)). However, the time-biased sampling data sets almost
285 invariably have posterior distributions with higher uncertainty than those from the time-uniform sampling
286 (fig. 5(b)), implying that the distribution of samples, and not just the number, is important for estimation
287 uncertainty.

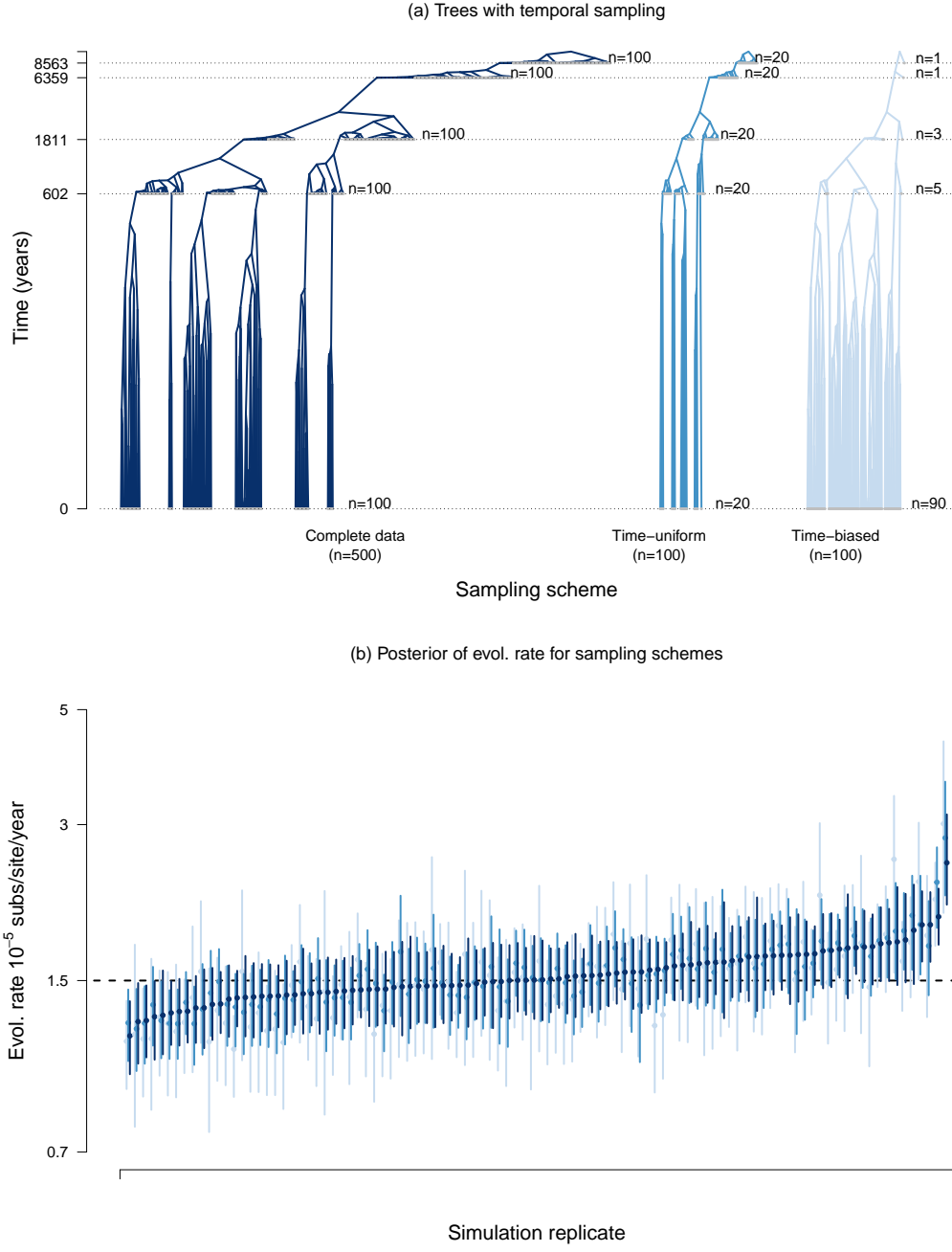


Figure 4: Analyses under sampling treatments over time. In (a) we show an example of the trees for a simulation replicate, with branch lengths and time in \log_{10} scale. The complete data set consists of 500 genome samples, collected in five points in time, with an equal number of samples per time point ($n=100$). The first sampling strategy is unbiased, where 20 samples are drawn from each time point, and is known here as ‘time-uniform’. The ‘time-biased’ regime is where sampling intensity decreases over time. Note that the total number of samples in the time-uniform and time-biased treatments is identical. In (b) we show the posterior estimates of the evolutionary rate for each treatment. Each simulation replicate is represented by three error bars: dark blue for the complete data, and lighter shades of blue for the estimates from the time-uniform and time-biased sampling treatments. The width of the error bars denotes the 95% quantile range and the dots are the mean value. The dashed line shows the true value used to generate the data.

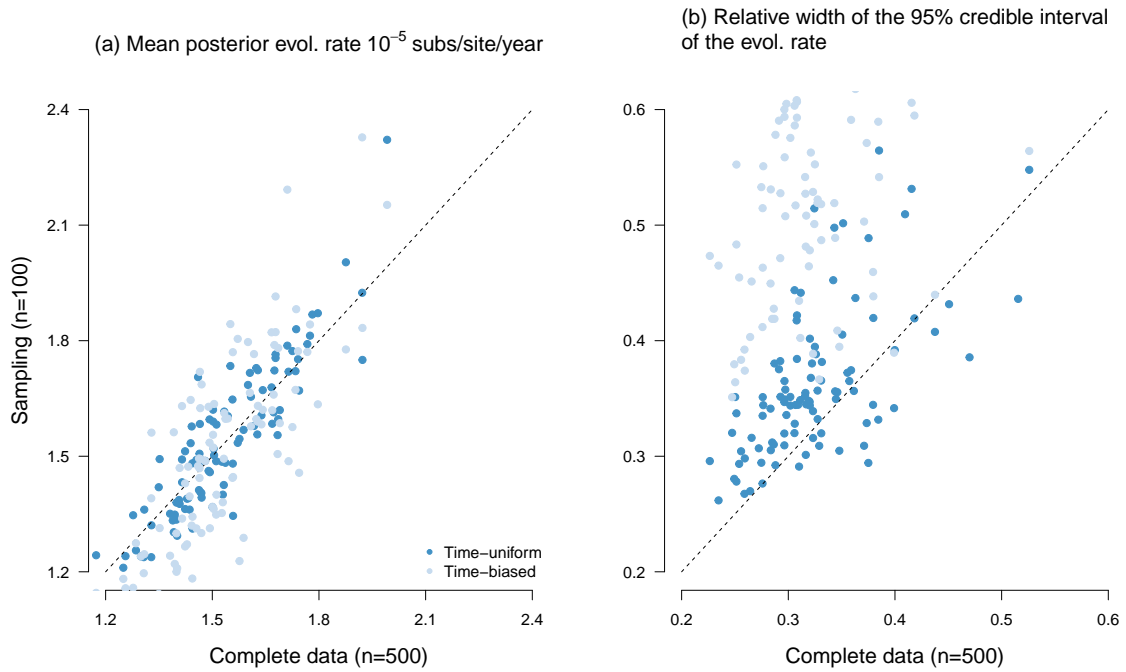


Figure 5: Comparison of posterior evolutionary rate estimates between complete data (x-axis) and two sampling treatments (y-axis): time-uniform (dark blue) and time-biased (light blue). Each dot is a simulation replicate. In (a) we show the mean posterior evolutionary rate estimate. Points that fall along the $y=x$ line (dashed line) represent identical mean posterior for the sampling treatment and the complete data, while those above or below represent higher or lower estimates, respectively, relative to the complete data. In (b) we show the width of the credible interval (a measure of precision or uncertainty), calculated as the upper minus the lower 95% credible interval range divided by the mean value. Values that fall along the $y=x$ line denote those for which the complete data and either sampling strategies are equally precise, while those above and below the $y=x$ line are more or less precise, respectively.

288 2.4 Empirical analyses of Hepatitis B virus (HBV) ancient and modern genomes

289 To explore the impact of the width of the sampling window and the temporal sampling bias on the estimates
 290 of evolutionary rates and times, we performed analyses of a HBV data set that includes modern and ancient
 291 genomes, from Kocher et al. (2021). The complete data set consisted of 232 genomes of length 3,344 nu-
 292 cleotides and with a sampling window of 10,535 years. HBV is an ancient pathogen that has likely codiverged
 293 with human populations for thousands of years (Locarnini et al., 2021, Mühlmann et al., 2018, Paraskevis
 294 et al., 2013, Zehender et al., 2014), and thus its phylodynamic threshold has been reached while it has not
 295 been empirically established if it can be considered to be a measurably evolving population, as is the case
 296 for recent outbreaks, like SARS-CoV-2 (Duchene et al., 2020a).

297 For our first set of analyses we varied the width of the sampling window. We drew 100 genomes with
 298 different sampling window widths: 0 (only modern samples), up to 500, 1,000, or 5,000 years before present.
 299 Increasing the sampling window resulted in estimates of the evolutionary rate that were more precise and
 300 closer to the estimate from the complete data set (fig. 6). Here we find that the evolutionary rate is estimated
 301 to be higher for shorter sampling windows, with correspondingly older estimates for the tree height. This

302 pattern can be due to one or a combination of other factors influencing the inference, for example the vagaries
 303 of evolutionary rate variation in this virus, particularly time-dependency (Vrancken et al., 2017). Similarly,
 304 population structure that is unaccounted for has been shown to produce an overestimation of the evolutionary
 305 rate, because under the tree prior samples that are genetically linked are expected to have been sampled at
 306 the same point in time (Möller et al., 2018).

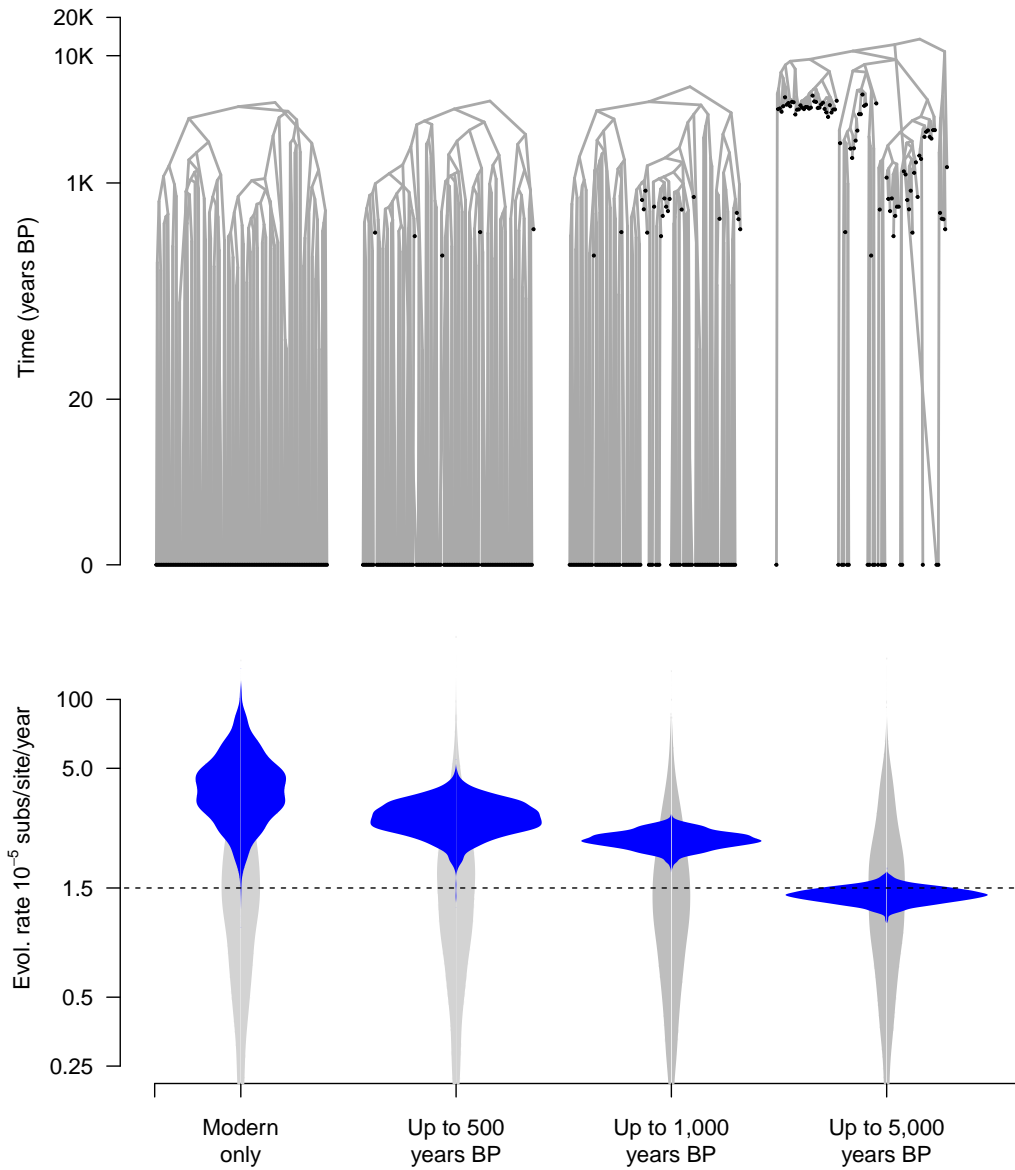


Figure 6: Results from empirical analyses of Hepatitis B virus (HBV) ancient DNA data. The phylogenetic trees correspond to highest clade credibility trees from three analyses where the data were subsampled to increase the width of the sampling window progressively. First, we only consider modern samples, then those up to 500, 1,000, and 5,000 years before present. In all cases the data sets consist of 100 genome samples. The violin plots show the posterior distribution of the evolutionary rate in blue and its corresponding prior in orange. The dashed line shows the mean evolutionary rate estimate from the complete data set.

307 For our second set of empirical analyses, we subsampled the data to produce a range of temporally biased
308 sampling scenarios. We varied the proportion of modern samples, from 95% to 10%. Here the sampling
309 window is constant because we always retain the most ancient samples. Each data set consisted of 100
310 genomes, such that they only differ in the distribution of modern and ancient samples (fig. 7).

311 The impact of temporal sampling bias was less clear than in our simulations above (figs 4 and 5). The data
312 set with 95% modern genomes had the highest uncertainty in the evolutionary rate estimate, but uncertainty
313 did not decrease monotonically with the proportion of modern genomes. Moreover, the posterior estimate of
314 the evolutionary rate from the data set with 50% modern genomes deviated the most from the that obtained
315 using the full data set. These results demonstrate that the exact impact of temporal sampling bias may be
316 difficult to predict in practice, but that generally increasing the number of ancient samples results in data
317 sets that are more informative, in that the difference between the prior and posterior is more pronounced
318 than when only a few ancient samples are available.

319 3 Discussion

320 The concepts of the phyloydamic threshold, measurably evolving populations, and temporal signal are
321 helpful for our understanding of rapidly evolving organisms or data sets with ancient DNA. Our analyses
322 help us disentangle the definition of these concepts and their practical implications. Our study concentrates
323 on the estimates of the evolutionary rate. Beyond its biological implications, this parameter is essential for
324 estimating evolutionary timescales. Our performance metrics for the age of the root-node are comparable to
325 those of the evolutionary rates (see Supplementary material online).

326 The phylodynamic threshold and measurable evolution are not discrete bounds. Increasing the sampling
327 window generally reduces uncertainty and improves accuracy (bias and coverage), but there is no clear cut-off
328 for when the estimates become accurate and objectively ‘precise’. Notably, the prior on the phylogenetic tree
329 and the evolutionary rate are particularly influential for estimating evolutionary rates and timescales (for a
330 detailed investigation see Tay et al. (2024)).

331 In fact, data sampled from a population that has attained its phylodynamic threshold does necessarily
332 mean that the resulting estimates will be correct. In these circumstances the phylodynamic threshold sim-
333 ply means that there is a measurable amount of genetic diversity within the sampling window. However,
334 our measures of coverage, uncertainty and bias for data with sampling windows of $0.5 \times$ the phylodynamic
335 threshold are often comparable to those obtained with much wider sampling windows, given that the prior
336 on the evolutionary rate prior is not substantially biased.

337 In the case that the prior is substantially biased a sampling widow of $100 \times$ the phylodynamic threshold
338 may be needed to reduce such bias. The extent to which we can draw inferences from data that have attained
339 the phylodynamic threshold or that are measurably evolving depends on the extent to which the data can
340 inform the posterior, which is ultimately a measure of the relative contribution of the prior and the data
341 (via the likelihood function). Our results suggest that using hierarchical priors may be an effective means of
342 minimising the biases due to a poorly chosen prior. We emphasise that a prior that imposes a downward bias
343 appears to be more problematic than one that favours high evolutionary rates. We attribute this to the fact
344 that the upper bound on the evolutionary rate is effectively bracketed by the sampling window. The maximum

345 evolutionary rate is the total genetic divergence divided by the sampling window width, whereas in principle
346 there is no bound on the age of a tree and thus the evolutionary rate can effectively reach zero (i.e. if time
347 tends to infinity). We note that the default prior on the evolutionary rate in population Bayesian phylogenetic
348 packages (e.g. BEAST2 and BEASTX (Baele et al., 2025)) is either a uniform distribution between 0 and
349 infinity or a CTMC rate reference prior (Ferreira and Suchard, 2008, Wang and Yang, 2014), both of which
350 tend to favour low evolutionary rate values, and should thus be considered carefully, particularly when the
351 sampling window is narrower than the phylodynamic threshold.

352 Ideally, the prior and posterior of key parameters, such as the height of the root or the evolutionary rate
353 should overlap, while the posterior should be narrower than the prior (i.e. more informative), meaning that
354 the data and the prior are not in conflict (for recent work on quantifying prior-data conflict see: Nott et al.
355 2020). In this vein, assessing the adequacy of the model and prior via predictive checks can be illuminating
356 (McElreath, 2018), especially in situations where the joint prior is poorly understood (see Baele and Lemey
357 2014, Wang and Yang 2014 for discussions about the prior in Bayesian phylogenetics). Recent years have seen
358 the development of a range of methods for assessing phylogenetic model adequacy (Brown and Thomson,
359 2018, Duchêne et al., 2018, Duchene et al., 2019, McElreath, 2018), for instance one can simulate phylogenetic
360 trees under the posterior estimates to verify whether the height of the root node and the topology could have
361 been generated by the model in question.

362 Measurably evolving populations are those for which the phylodynamic threshold has been attained and
363 the sampling window is *sufficiently* wide. The criteria for determining the phylodynamic threshold and
364 whether a population is measurably evolving are the same, and are typically assessed via temporal signal.
365 Statistical tests for this purpose quantify the strength of the association between sampling times and genetic
366 distance (Duchêne et al., 2015, Featherstone et al., 2024, Murray et al., 2016, Rambaut et al., 2016, Rieux
367 and Balloux, 2016). That is, the degree to which the sampling times on their own constitute an informative
368 molecular clock calibration. We contend that assessing prior sensitivity is more important than the outcome
369 of tests of temporal signal for obtaining reliable molecular clock estimates. In fact, a poor choice of prior
370 can mislead tests of temporal signal (Tay et al., 2024). If data are drawn from a sampling window that
371 spans the expected phylodynamic threshold, the presence of temporal signal is likely supported by most
372 tests, suggesting accurate estimates. Yet, if the prior used for the estimation is misleading and informative,
373 it might actually obscure the ‘correct’ signal from the data. In contrast, if the data are drawn from a narrow
374 sampling window but the prior is reasonable then the estimates may be still be reliable, despite a lack of
375 temporal signal. It also has to be noted that an increasing sampling effort does not necessarily lead to
376 increasingly correct inferences, because misspecification not only in prior distributions of hyper-parameters,
377 but also in the underlying model, can introduce biases (Ferretti et al., 2024, Möller et al., 2018).

378 An obvious concern about molecular clock calibrations using sequence sampling times is sampling bias.
379 We find that temporal sampling bias, where data are overwhelmingly collected at a particular period of
380 time does not have a substantial impact in estimation accuracy on a simple coalescent model, but that
381 increasing the number of ancient sequences can reduce uncertainty. An other form of sampling bias is when
382 genetic diversity is not uniformly sampled or the underlying population is structured. Previous work has
383 demonstrated that in such cases, the evolutionary rate and the age of the root node tend to be overestimated
384 (Möller et al., 2018), a problem that diminishes when sequence data are increasingly informative or by using

385 a tree prior that explicitly models population structure (e.g. Kühnert et al. 2016, Müller et al. 2017).

386 Our study has a few limitations that have been partly addressed elsewhere. The number of sequences
387 is fixed in most of our experiments, but it is well known that increasing the number of sequences generally
388 means that data are more informative and thus the estimates are more precise (see Möller et al. (2018) and
389 our fig. 4), and therefore it is likely that the width of the sampling window needed to obtain reliable estimates
390 also depends on the number of sequences. Moreover, our simulation experiments involved a low degree of
391 evolutionary rate variation among lineages. In this respect, it is expected that the width of the sampling
392 window scales with the amount of dispersion in the molecular clock. In addition, our simulations are based
393 on a simple population dynamic model, the constant coalescent. The impact of the sampling scheme and
394 width is likely to be more complex for models with more parameters. We also assume the correct model of
395 evolution and population growth in all simulation-based inferences. With the empirical analysis, we, however,
396 highlight how conclusions drawn from these do not directly extend to real-world data. Rather, the isolated
397 effects found therein describe only one of many elements impacting the inference from real data. Further
398 scrutiny of these factors is warranted, but the main implication is that the necessary sampling time window
399 is combination of the data set, the organism, and the model at hand.

400 Overall, our study elucidates some of the fundamental intricacies of molecular clock calibration strategies.
401 We urge researchers to carefully question their model and its underlying prior assumptions, not only via tests
402 of temporal signal, but also through careful choice of the prior, an understanding of the information content
403 in the data, and the implications of model misspecification.

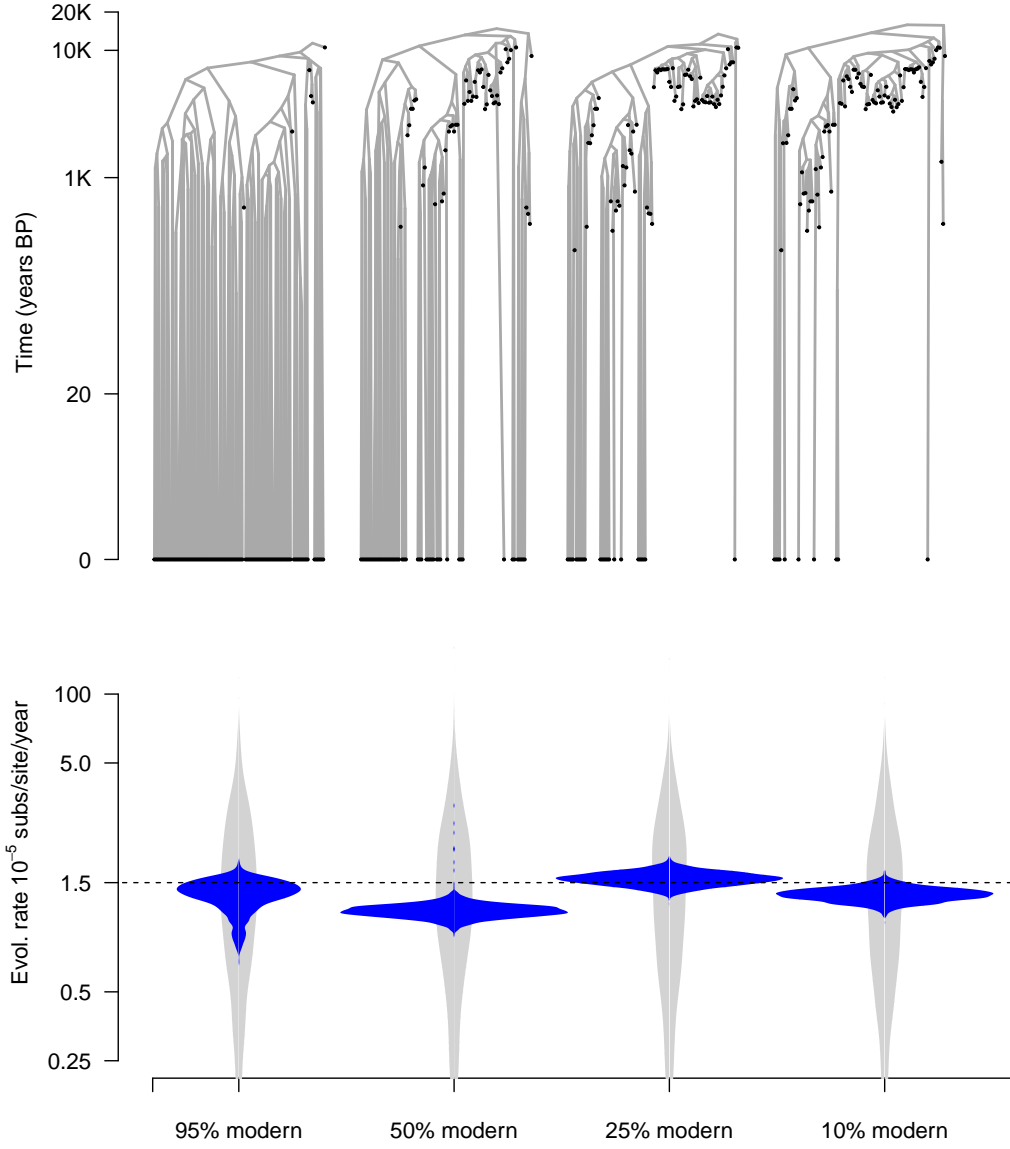


Figure 7: Results from empirical analyses of Hepatitis B virus (HBV) ancient DNA data. The phylogenetic trees correspond to highest clade credibility trees from three analyses where the data were subsampled to include an increasing number of ancient samples. First, we consider a data set for which the samples are 95% modern and the remaining 5% being the most ancient. Then, we reduce the number of modern samples to 50%, 25% and 10%, and the rest being ancient. Note that the sampling window is constant because we always retain the most ancient samples. In all cases the data sets consist of 100 genome samples. The violin plots show the posterior distribution of the evolutionary rate in blue and its corresponding prior in orange. The dashed line shows the mean evolutionary rate estimate from the complete data set.

404 **4 Materials and methods**

405 **4.1 Simulations**

406 **4.1.1 Data generation**

407 We simulated phylogenetic trees and the evolution of nucleotide sequences to assess the impact of varying
408 the sampling window and temporal sampling bias. We parameterised our simulations to resemble an HBV
409 population evolving over 10,000 years before present, as described by Kocher et al. (2021).

410 We generated phylogenetic trees under a coalescent process in which the population size has been constant
411 over time using the package ReMaster (Vaughan, 2024), part of the BEAST 2 (version 2.7) software. We set
412 the population size to 5,000, which results in trees with an average age of about 10,000 time units (years)
413 (see Arbisser et al. 2018). The number of samples (i.e. tips) drawn from the trees and their ages was defined
414 in ReMaster, according to the simulation scenario described below.

415 The simulation of sequence data requires trees with branch lengths in units of subs/site, instead of time.
416 For this purpose, we multiplied the branch lengths of the simulated time tree with the rate of evolution,
417 a lognormally distributed random variable with parameters $\mu = \log(1.5 \times 10^{-5}) - \frac{0.25^2}{2}$ and $\sigma = 0.25$.
418 This procedure equates to simulating an uncorrelated relaxed molecular clock model with an underlying
419 lognormal distribution (Drummond et al., 2006) with mean, M of 1.5×10^{-5} subs/site/year and a standard
420 deviation of 0.25 subs/site/year (following that $\mu = \log(M) - \frac{\sigma^2}{2}$). Because we multiply the branch lengths
421 in units of years by a variable in subs/site/year, the resulting trees have branch lengths in units of subs/site,
422 formally known as phylogenograms, in contrast to chronograms where the branch lengths correspond to time.
423 We obtained sequence alignments using the R package phangorn (v2.8.1) (Schliep, 2011), according to a
424 HKY+ Γ_4 substitution model, with parameters $\kappa = 2$, $\alpha = 4$, and equal base frequencies. The alignments
425 consisted of 3,200 nucleotides to match the average genome size of HBV.

426 We considered the expected phylodynamic threshold of our data to be about 20 years. For our simulations
427 where we varied the sampling window, we set the ages of 100 tips to be sampled at present (all have an age
428 of 0), or to be drawn from a uniform distribution between 0 and 10 (1/2 of the expected phylodynamic
429 threshold), 0 and 20, 0 and 200, or 0 and 2,000.

430 To investigate the impact of temporal sampling bias we initially simulated trees with 500 tips with
431 sampling times distributed in 5 time points, with 100 tips per time point. The distribution of sampling times
432 followed an exponential distribution with mean of 4,000, such that sampling times were concentrated towards
433 the present. We simulated these complete trees in ReMaster. We followed the procedure above to simulate
434 a molecular clock model and sequence alignments.

435 We conducted two sampling schemes for the trees with 500 tips: the ‘time-uniform’ scheme consisted
436 of drawing 20 samples from each time point, whereas the ‘time-biased’ scheme included of mostly modern
437 samples (90 from the present, and 5, 3, 1, and 1 from the remaining time points). For each simulation
438 scenario we generated 100 replicates.

439 **4.1.2 Analysis of simulated data**

440 We analysed all data sets in BEAST 2 under a model that matched that used to generate the data: the
 441 HKY+ Γ_4 substitution model, a uncorrelated relaxed molecular clock model with an underlying lognormal
 442 distribution, and a constant size coalescent tree prior. We used the default prior configuration in the program,
 443 except for the mean evolutionary rate (M) and the population size of the coalescent (N , where $N = N_e \times \tau$,
 444 where N_e is the effective population size and τ is generation time). For the population size we assumed
 445 $N \sim \text{Exponential}(\text{mean} = 5,000)$, which is centred in the value used to generate the data. The expected
 446 height of the root node is roughly 10,000 years (expected time to coalescent = $2 \times N$ for an ultrametric tree,
 447 see Nordborg (2019)).

448 For the mean evolutionary rate we considered a range of priors with different degrees of information
 449 content (uncertainty) and for which the mean was either the value used to generate the data, or one order of
 450 magnitude higher or lower, as shown in table ???. We also included three degrees of uncertainty in such prior
 451 distributions, where the 95% quantile width was equal to the mean, or around three or six times as wide. In
 452 all cases we set the sampling times for calibration.

453 In the case of ultrametric trees, sampling times are set to the present, such that all calibration information
 454 is provided by the tree prior. Concretely, let the tree length in time (sum of all branch lengths t_i in units
 455 of time) be T_t , the tree height in units of time T_h , the branch rates r_i (the vector of branch rates $\vec{R} \in$
 456 $\{r_1, \dots, r_{\text{num. branches}}\}$ (see Douglas et al. 2021), and T_d is the tree length in genetic divergence (sum of branch
 457 lengths d_i in subs/site).

458 In most Bayesian phylogenetic frameworks branch lengths in genetic distance are the product of rates and
 459 times (Douglas et al., 2021, Drummond et al., 2006), such that $T_d = \sum d_i = \sum r_i t_i$. Importantly, T_d is given
 460 by the phylogenetic likelihood and only depends on genetic distance and substitution model parameters.
 461 The average evolutionary rate (an estimate of parameter M), $\bar{r} = \frac{\sum r_i t_i}{\sum t_i} = \frac{T_d}{T_t}$. However, T_t is a function
 462 of population size N through $\mathbb{E}[T_t] = 2 \times N \times \log(n)$, where n is the number of sampled lineages (Arbisser
 463 et al., 2018, Tavaré et al., 1997). Thus, the prior on N affects T_h (through $\mathbb{E}[T_h] = 2 \times N(1 - \frac{1}{n}) \approx 2 \times N$ for
 464 large n), T_t , and the average evolutionary rate ($\bar{r} = \frac{T_d}{2 \times N \times \log(n)}$, where T_d is independent of time).

We used an additional configuration for the prior M using a hierarchical structure as follows:

$$M \sim \text{Gamma}(\text{shape}, \text{rate})$$

$$\text{shape} \sim \text{LogNormal}(1, 5)$$

$$\text{rate} \sim \text{LogNormal}(1, 5)$$

465 To set up this model, we simply treat the *shape* and *rate* as parameters that are sampled in the model.

466 We used Markov chain Monte Carlo (MCMC) to sample the posterior distribution for all analyses. We
 467 set the chain length to 10^8 steps, sampling every 5×10^4 steps. We deemed sufficient sampling by verifying
 468 that the effective sample size was at least 200, by using the R package CODA (version 0.19) (Plummer et al.,
 469 2006). When this criterion was not met we extended the chain length to 5×10^8 steps.

470 To visualise the prior on M in our model with a hierarchical prior we drew MCMC samples from the
 471 marginal prior of M . That is, the prior integrating over the hyperprior distributions and all other parameters.

472 We obtained such samples by setting the option `sampleFromPrior="true"` in the input xml files in BEAST
473 2, which conducts the MCMC while ignoring the phylogenetic likelihood.

474 **4.1.3 HBV empirical data**

475 We selected a complete genome data set of HBV published by Kocher et al. (2021). The complete alignment
476 included 232 genomes of length 3,344 nucleotides, with 1,807 variable sites, and 1,498 site patterns. The
477 sampling times ranged from the present to 10,535 years before present. To investigate the impact of varying
478 the sampling window and on temporal sampling bias we subsampled the data as described in our Results
479 section. We analysed each data set using the same model and prior settings as in our simulations, including
480 the use of the reasonable and misleading prior configuration.

481 **5 Data availability**

482 Computer code, analysis files, and data sets in this study are available at:

483 https://github.com/sebastianduchene/phylo_threshold_code_data

484 **6 Competing interests**

485 None.

486 **7 Acknowledgments**

487 Pending.

488 **8 Funding**

489 This work received funding from the Inception program (Investissement d’Avenir grant ANR-16-CONV-0005
490 awarded to SD) and the Australian National Health and Medical Research Council (2017284 awarded to SD),

491 **References**

492 A. Andrades Valtueña, G. U. Neumann, M. A. Spyrou, L. Musralina, F. Aron, A. Beisenov, A. B. Belinskiy,
493 K. I. Bos, A. Buzhilova, M. Conrad, et al. Stone age yersinia pestis genomes shed light on the early
494 evolution, diversity, and ecology of plague. *Proceedings of the National Academy of Sciences*, 119(17):
495 e2116722119, 2022.

496 I. M. Arbisser, E. M. Jewett, and N. A. Rosenberg. On the joint distribution of tree height and tree length
497 under the coalescent. *Theoretical population biology*, 122:46–56, 2018.

498 G. Baele and P. Lemey. Bayesian model selection in phylogenetics and genealogy-based population genetics.
499 In M. Chen, K. L, and L. PO, editors, *Bayesian phylogenetics, methods, algorithms, and applications*,
500 chapter 4, pages 59–93. CPC Press, Boca Raton (Florida), 2014.

- 501 G. Baele, X. Ji, G. W. Hassler, J. T. McCrone, Y. Shao, Z. Zhang, A. J. Holbrook, P. Lemey, A. J. Drummond,
502 A. Rambaut, et al. Beast x for bayesian phylogenetic, phylogeographic and phylodynamic inference. *Nature*
503 *Methods*, 22(8):1653–1656, 2025.
- 504 R. Biek, O. G. Pybus, J. O. Lloyd-Smith, and X. Didelot. Measurably evolving pathogens in the genomic
505 era. *Trends in ecology & evolution*, 30(6):306–313, 2015.
- 506 M. F. Boni, P. Lemey, X. Jiang, T. T.-Y. Lam, B. W. Perry, T. A. Castoe, A. Rambaut, and D. L. Robertson.
507 Evolutionary origins of the sars-cov-2 sarbecovirus lineage responsible for the covid-19 pandemic. *Nature*
508 *microbiology*, 5(11):1408–1417, 2020.
- 509 R. Bouckaert, T. G. Vaughan, J. Barido-Sottani, S. Duchêne, M. Fourment, A. Gavryushkina, J. Heled,
510 G. Jones, D. Kühnert, N. De Maio, et al. Beast 2.5: An advanced software platform for bayesian evolu-
511 tionary analysis. *PLoS computational biology*, 15(4):e1006650, 2019.
- 512 L. Bromham, S. Duchêne, X. Hua, A. M. Ritchie, D. A. Duchêne, and S. Y. Ho. Bayesian molecular dating:
513 opening up the black box. *Biological Reviews*, 93(2):1165–1191, 2018.
- 514 J. M. Brown and R. C. Thomson. Evaluating model performance in evolutionary biology. *Annual Review of*
515 *Ecology, Evolution, and Systematics*, 49(1):95–114, 2018.
- 516 D. A. Buonagurio, S. Nakada, J. D. Parvin, M. Krystal, P. Palese, and W. M. Fitch. Evolution of human
517 influenza a viruses over 50 years: rapid, uniform rate of change in ns gene. *Science*, 232(4753):980–982,
518 1986.
- 519 A. M. Devault, G. B. Golding, N. Waglechner, J. M. Enk, M. Kuch, J. H. Tien, M. Shi, D. N. Fisman, A. N.
520 Dhody, S. Forrest, et al. Second-pandemic strain of vibrio cholerae from the philadelphia cholera outbreak
521 of 1849. *New England Journal of Medicine*, 370(4):334–340, 2014.
- 522 M. Dos Reis and Z. Yang. The unbearable uncertainty of bayesian divergence time estimation. *Journal of*
523 *Systematics and Evolution*, 51(1):30–43, 2013.
- 524 J. Douglas, R. Zhang, and R. Bouckaert. Adaptive dating and fast proposals: Revisiting the phylogenetic
525 relaxed clock model. *PLoS computational biology*, 17(2):e1008322, 2021.
- 526 A. Drummond, O. G. Pybus, and A. Rambaut. Inference of viral evolutionary rates from molecular sequences.
527 *Adv Parasitol*, 54:331–358, 2003a.
- 528 A. J. Drummond, O. G. Pybus, A. Rambaut, R. Forsberg, and A. G. Rodrigo. Measurably evolving popu-
529 lations. *Trends in ecology & evolution*, 18(9):481–488, 2003b.
- 530 A. J. Drummond, S. Y. W. Ho, M. J. Phillips, and A. Rambaut. Relaxed phylogenetics and dating with
531 confidence. *PLoS Biology*, 4(5):e88, 2006.
- 532 D. A. Duchêne, S. Duchêne, and S. Y. Ho. Phylomad: efficient assessment of phylogenomic model adequacy.
533 *Bioinformatics*, 34(13):2300–2301, 2018.

- 534 S. Duchêne, R. Lanfear, and S. Y. Ho. The impact of calibration and clock-model choice on molecular
535 estimates of divergence times. *Molecular phylogenetics and evolution*, 78:277–289, 2014.
- 536 S. Duchêne, D. Duchêne, E. C. Holmes, and S. Y. Ho. The performance of the date-randomization test in
537 phylogenetic analyses of time-structured virus data. *Molecular Biology and Evolution*, 32(7):1895–1906,
538 2015.
- 539 S. Duchene, K. E. Holt, F.-X. Weill, S. Le Hello, J. Hawkey, D. J. Edwards, M. Fourment, and E. C. Holmes.
540 Genome-scale rates of evolutionary change in bacteria. *Microbial genomics*, 2(11):e000094, 2016.
- 541 S. Duchene, D. A. Duchene, J. L. Geoghegan, Z. A. Dyson, J. Hawkey, and K. E. Holt. Inferring demographic
542 parameters in bacterial genomic data using bayesian and hybrid phylogenetic methods. *BMC evolutionary
543 biology*, 18:1–11, 2018.
- 544 S. Duchene, R. Bouckaert, D. A. Duchene, T. Stadler, and A. J. Drummond. Phylodynamic model adequacy
545 using posterior predictive simulations. *Systematic biology*, 68(2):358–364, 2019.
- 546 S. Duchene, L. Featherstone, M. Haritopoulou-Sinanidou, A. Rambaut, P. Lemey, and G. Baele. Temporal
547 signal and the phylodynamic threshold of sars-cov-2. *Virus evolution*, 6(2):veaa061, 2020a.
- 548 S. Duchene, S. Y. Ho, A. G. Carmichael, E. C. Holmes, and H. Poinar. The recovery, interpretation and use
549 of ancient pathogen genomes. *Current Biology*, 30(19):R1215–R1231, 2020b.
- 550 S. Duchene, P. Lemey, T. Stadler, S. Y. Ho, D. A. Duchene, V. Dhanasekaran, and G. Baele. Bayesian
551 evaluation of temporal signal in measurably evolving populations. *Molecular Biology and Evolution*, 37
552 (11):3363–3379, 2020c.
- 553 K. Eaton, L. Featherstone, S. Duchene, A. G. Carmichael, N. Varlik, G. B. Golding, E. C. Holmes, and
554 H. N. Poinar. Plagued by a cryptic clock: insight and issues from the global phylogeny of yersinia pestis.
555 *Communications Biology*, 6(1):23, 2023.
- 556 V. Eldholm, J. Monteserin, A. Rieux, B. Lopez, B. Sobkowiak, V. Ritacco, and F. Balloux. Four decades of
557 transmission of a multidrug-resistant mycobacterium tuberculosis outbreak strain. *Nature communications*,
558 6(1):7119, 2015.
- 559 L. A. Featherstone, A. Rambaut, S. Duchene, and W. Wirth. Clockor2: Inferring global and local strict
560 molecular clocks using root-to-tip regression. *Systematic biology*, 73(3):623–628, 2024.
- 561 M. A. Ferreira and M. A. Suchard. Bayesian analysis of elapsed times in continuous-time markov chains.
562 *Canadian Journal of Statistics*, 36(3):355–368, 2008.
- 563 L. Ferretti, T. Golubchik, F. Di Lauro, M. Ghafari, J. Villabona-Arenas, K. E. Atkins, C. Fraser, and M. Hall.
564 Biased estimates of phylogenetic branch lengths resulting from the discretised gamma model of site rate
565 heterogeneity. *bioRxiv*, pages 2024–08, 2024.
- 566 A. Gavryushkina, T. A. Heath, D. T. Ksepka, T. Stadler, D. Welch, and A. J. Drummond. Bayesian total-
567 evidence dating reveals the recent crown radiation of penguins. *Systematic biology*, 66(1):57–73, 2017.

- 568 M. Ghafari, L. du Plessis, J. Raghwani, S. Bhatt, B. Xu, O. G. Pybus, and A. Katzourakis. Purifying selec-
569 tion determines the short-term time dependency of evolutionary rates in sars-cov-2 and ph1n1 influenza.
570 *Molecular Biology and Evolution*, 39(2):msac009, 2022.
- 571 N. Gharbi, E. Rousseau, and T. Wirth. Clock rates and bayesian evaluation of temporal signal. In *Phyloge-
572 nomics*, pages 153–175. Elsevier, 2024.
- 573 T. Gojobori, E. N. Moriyama, and M. Kimura. Molecular clock of viral evolution, and the neutral theory.
574 *Proceedings of the National Academy of Sciences*, 87(24):10015–10018, 1990.
- 575 S. Guindon. Rates and rocks: strengths and weaknesses of molecular dating methods. *Frontiers in Genetics*,
576 11:526, 2020.
- 577 T. A. Heath, J. P. Huelsenbeck, and T. Stadler. The fossilized birth–death process for coherent calibration of
578 divergence-time estimates. *Proceedings of the National Academy of Sciences*, 111(29):E2957–E2966, 2014.
- 579 S. Y. Ho. The changing face of the molecular evolutionary clock. *Trends in Ecology & Evolution*, 29(9):
580 496–503, 2014.
- 581 S. Y. Ho and S. Duchêne. Molecular-clock methods for estimating evolutionary rates and timescales. *Molecular
582 Ecology*, 23(24):5947–5965, 2014.
- 583 G. Kahila Bar-Gal, M. J. Kim, A. Klein, D. H. Shin, C. S. Oh, J. W. Kim, T.-H. Kim, S. B. Kim, P. R.
584 Grant, O. Pappo, et al. Tracing hepatitis b virus to the 16th century in a korean mummy. *Hepatology*, 56
585 (5):1671–1680, 2012.
- 586 A. Kocher, L. Papac, R. Barquera, F. M. Key, M. A. Spyrou, R. Hübler, A. B. Rohrlach, F. Aron, R. Stahl,
587 A. Wissgott, et al. Ten millennia of hepatitis b virus evolution. *Science*, 374(6564):182–188, 2021.
- 588 D. Kühnert, T. Stadler, T. G. Vaughan, and A. J. Drummond. Phylodynamics with migration: a computa-
589 tional framework to quantify population structure from genomic data. *Molecular biology and evolution*, 33
590 (8):2102–2116, 2016.
- 591 D. Kühnert, M. Coscolla, D. Brites, D. Stucki, J. Metcalfe, L. Fenner, S. Gagneux, and T. Stadler. Tuber-
592 culosis outbreak investigation using phylodynamic analysis. *Epidemics*, 25:47–53, 2018.
- 593 S. A. Locarnini, M. Littlejohn, and L. K. Yuen. Origins and evolution of the primate hepatitis b virus.
594 *Frontiers in Microbiology*, 12:653684, 2021.
- 595 R. McElreath. *Statistical rethinking: A Bayesian course with examples in R and Stan*. Chapman and
596 Hall/CRC, 2018.
- 597 F. Menardo, S. Duchêne, D. Brites, and S. Gagneux. The molecular clock of mycobacterium tuberculosis.
598 *PLoS pathogens*, 15(9):e1008067, 2019.
- 599 F. K. Mendes, R. Bouckaert, L. M. Carvalho, and A. J. Drummond. How to validate a bayesian evolutionary
600 model. *Systematic Biology*, 74(1):158–175, 2025.

- 601 M. Merker, J.-P. Rasigade, M. Barbier, H. Cox, S. Feuerriegel, T. A. Kohl, E. Shitikov, K. Klaos, C. Gaudin,
602 R. Antoine, et al. Transcontinental spread and evolution of mycobacterium tuberculosis w148 european/russian clade toward extensively drug resistant tuberculosis. *Nature Communications*, 13(1):5105,
603 2022.
- 605 S. Möller, L. du Plessis, and T. Stadler. Impact of the tree prior on estimating clock rates during epidemic
606 outbreaks. *Proceedings of the National Academy of Sciences*, 115(16):4200–4205, 2018.
- 607 B. Mühlmann, T. C. Jones, P. d. B. Damgaard, M. E. Allentoft, I. Shevnina, A. Logvin, E. Usmanova, I. P.
608 Panyushkina, B. Boldgiv, T. Bazartseren, et al. Ancient hepatitis b viruses from the bronze age to the
609 medieval period. *Nature*, 557(7705):418–423, 2018.
- 610 N. F. Müller, D. A. Rasmussen, and T. Stadler. The structured coalescent and its approximations. *Molecular
611 biology and evolution*, 34(11):2970–2981, 2017.
- 612 G. G. Murray, F. Wang, E. M. Harrison, G. K. Paterson, A. E. Mather, S. R. Harris, M. A. Holmes,
613 A. Rambaut, and J. J. Welch. The effect of genetic structure on molecular dating and tests for temporal
614 signal. *Methods in Ecology and Evolution*, 7(1):80–89, 2016.
- 615 M. Nordborg. Coalescent theory. *Handbook of Statistical Genomics: Two Volume Set*, pages 145–30, 2019.
- 616 D. J. Nott, X. Wang, M. Evans, and B.-G. Englert. Checking for prior-data conflict using prior-to-posterior
617 divergences. *Statistical Science*, 35(2):234–253, 2020.
- 618 D. Paraskevis, G. Magiorkinis, E. Magiorkinis, S. Y. Ho, R. Belshaw, J.-P. Allain, and A. Hatzakis. Dating
619 the origin and dispersal of hepatitis b virus infection in humans and primates. *Hepatology*, 57(3):908–916,
620 2013.
- 621 M. Plummer, N. Best, K. Cowles, K. Vines, et al. Coda: convergence diagnosis and output analysis for
622 mcmc. *R news*, 6(1):7–11, 2006.
- 623 A. Rambaut, T. T. Lam, L. Max Carvalho, and O. G. Pybus. Exploring the temporal structure of heterochronous sequences using tempest (formerly path-o-gen). *Virus evolution*, 2(1):vew007, 2016.
- 625 C. Ramsden, E. C. Holmes, and M. A. Charleston. Hantavirus evolution in relation to its rodent and
626 insectivore hosts: no evidence for codivergence. *Molecular biology and evolution*, 26(1):143–153, 2009.
- 627 A. Rieux and F. Balloux. Inferences from tip-calibrated phylogenies: a review and a practical guide. *Molecular
628 ecology*, 25(9):1911–1924, 2016.
- 629 F. Ronquist, N. Lartillot, and M. J. Phillips. Closing the gap between rocks and clocks using total-evidence
630 dating. *Philosophical Transactions of the Royal Society B: Biological Sciences*, 371(1699):20150136, 2016.
- 631 Z. P. Ross, J. Klunk, G. Fornaciari, V. Giuffra, S. Duchêne, A. T. Duggan, D. Poinar, M. W. Douglas, J.-S.
632 Eden, E. C. Holmes, et al. The paradox of hbv evolution as revealed from a 16th century mummy. *PLoS
633 pathogens*, 14(1):e1006750, 2018.

- 634 R. Sanjuán. From molecular genetics to phydynamics: evolutionary relevance of mutation rates across
635 viruses. *PLoS pathogens*, 8(5):e1002685, 2012.
- 636 K. P. Schliep. phangorn: phylogenetic analysis in r. *Bioinformatics*, 27(4):592–593, 2011.
- 637 M. A. Spyrou, K. I. Bos, A. Herbig, and J. Krause. Ancient pathogen genomics as an emerging tool for
638 infectious disease research. *Nature Reviews Genetics*, 20(6):323–340, 2019a.
- 639 M. A. Spyrou, M. Keller, R. I. Tukhbatova, C. L. Scheib, E. A. Nelson, A. Andrades Valtueña, G. U.
640 Neumann, D. Walker, A. Alterauge, N. Carty, et al. Phylogeography of the second plague pandemic
641 revealed through analysis of historical yersinia pestis genomes. *Nature communications*, 10(1):4470, 2019b.
- 642 S. Tavaré, D. J. Balding, R. C. Griffiths, and P. Donnelly. Inferring coalescence times from dna sequence
643 data. *Genetics*, 145(2):505–518, 1997.
- 644 J. H. Tay, A. Kocher, and S. Duchene. Assessing the effect of model specification and prior sensitivity on
645 bayesian tests of temporal signal. *PLoS Computational Biology*, 20(11):e1012371, 2024.
- 646 N. S. Trovão, G. Baele, B. Vrancken, F. Bielejec, M. A. Suchard, D. Fargette, and P. Lemey. Host ecology
647 determines the dispersal patterns of a plant virus. *Virus evolution*, 1(1):vev016, 2015.
- 648 T. G. Vaughan. Remaster: improved phydodynamic simulation for beast 2.7. *Bioinformatics*, 40(1):btae015,
649 2024.
- 650 B. Vrancken, M. A. Suchard, and P. Lemey. Accurate quantification of within-and between-host hbv evolu-
651 tionary rates requires explicit transmission chain modelling. *Virus Evolution*, 3(2):vex028, 2017.
- 652 Y. Wang and Z. Yang. Priors in bayesian phylogenetics. *Bayesian phylogenetics: methods, algorithms, and*
653 *applications*, pages 5–24, 2014.
- 654 R. C. Warnock, Z. Yang, and P. C. Donoghue. Exploring uncertainty in the calibration of the molecular
655 clock. *Biology letters*, 8(1):156–159, 2012.
- 656 G. Zehender, E. Ebranati, E. Gabanelli, C. Sorrentino, A. L. Presti, E. Tanzi, M. Ciccozzi, and M. Galli.
657 Enigmatic origin of hepatitis b virus: an ancient travelling companion or a recent encounter? *World*
658 *Journal of Gastroenterology: WJG*, 20(24):7622, 2014.
- 659 E. Zuckerkandl and L. Pauling. Evolutionary divergence and convergence in proteins. In *Evolving genes and*
660 *proteins*, pages 97–166. Elsevier, 1965.